INTERNATIONAL JOURNAL OF CLIMATOLOGY
Int. J. Climatol. **23**: 1549–1566 (2003)
Published online in Wiley InterScience (www.interscience.wiley.com). DOI: 10.1002/joc.963

VARIABILITY OF THE IMPACT OF EL NIÑO–SOUTHERN OSCILLATION ON SEA-LEVEL PRESSURE ANOMALIES OVER THE NORTH ATLANTIC IN JANUARY TO MARCH (1874–1996)

I. GOUIRAND[a,b] and V. MORON[a,b]*
[a] *UFR des Sciences géographiques et de l'aménagement, Université de Provence (Aix–Marseille I), Aix en Provence, France*
[b] *CEREGE UMR-CNRS 6635, Aix en Provence, France*

Received 3 December 2002
Revised 23 July 2003
Accepted 10 August 2003

ABSTRACT

Sea-level pressure (SLP) anomalies over the North Atlantic and European (NAE) sector (25–70 °N, 100 °W–50 °E) and over a larger domain encompassing the entire North Pacific domain are studied to demonstrate that SLP anomalies (SLPAs) during boreal winter (January–March) vary widely between years characterized by the same El Niño–southern oscillation (ENSO) phase. The typical cold ENSO signal tends to be more stable than the warm one during the 1874–1996 period. The typical cold ENSO pattern (e.g. positive SLPA south of 55 °N across the North Atlantic and negative SLPA in the northern North Atlantic) is similar to the positive phase of the North Atlantic oscillation (NAO) and occurs throughout the 20th century, except during the 1950s and 1960s when the basinwide westerlies are particularly slow. On the contrary, the typical warm ENSO pattern (e.g. positive SLPA from central Canada to Scandinavia and negative SLPA from the southeastern USA to central Europe, corresponding to the negative phase of the NAO) occurs mainly from 1930 to 1970. Another robust warm ENSO pattern is associated with a large positive (negative) SLPA between Newfoundland and western Europe (between Greenland and Scandinavia), and occurs mainly at the beginning and the end of the 20th century when the basinwide North Atlantic westerlies are strengthened. All these patterns stay statistically significant when the multi-decadal variability is removed from the North Atlantic SLPA. It is shown that the low-frequency variability of the north tropical Atlantic sea-surface temperature anomalies could exert a modulating effect on the ENSO teleconnection. NAE SLPAs tend to be strong during warm (cold) ENSO winters and consistent with a negative (positive) phase of the NAO when the north tropical Atlantic is anomalously warm (cold). Lastly, the magnitude of the SLPA patterns over the NAE sector appears poorly related to the intensity of sea-surface temperature anomalies in the central and eastern equatorial Pacific. Copyright © 2003 Royal Meteorological Society.

KEY WORDS: El Niño–southern oscillation; surface atmospheric variability; North Atlantic; North Pacific; Europe; North America; boreal winter

1. INTRODUCTION

This paper focuses on the inter-event variability of sea-level pressure (SLP) anomalies associated with El Niño–southern oscillation (ENSO) over the North Atlantic and European (NAE) domain in January–March (JFM) during the period 1874–1996. ENSO is the major source of global climate anomalies (i.e. Ropelewski and Halpert, 1987, 1989, 1996; Kiladis and Diaz, 1989; Halpert and Ropelewski, 1992; Yulaeva and Wallace, 1994; Diaz *et al*., 2001) and is characterized by a quasi-periodic shift in sea-surface temperatures (SSTs) in the central and eastern equatorial Pacific Ocean, usually accompanied by a change in the southern oscillation (Philander, 1990). There are two distinct phases: a warm (cold) phase characterized by strong positive (negative) SST anomaly (SSTA) in the central and eastern equatorial Pacific Ocean (Philander, 1990). Our study covers the 30 warmest and coldest ENSO events from 1874 to 1996. The effects of warm

* Correspondence to: V. Moron, CEREGE, UMR-6635 CNRS, Europôle Méditérranéen de l'Arbois, BP80, 13545 Aix en Provence, France; e-mail: moron@cerege.fr

and cold ENSO events are felt almost everywhere during boreal winter, especially throughout the tropical zone (Ropelewski and Halpert, 1987, 1989, 1996; Kiladis and Diaz, 1989; Halpert and Ropelewski, 1992; Yulaeva and Wallace, 1994; Diaz *et al*., 2001). The most prominent impact of ENSO on Northern Hemisphere atmospheric circulation is related to the Pacific–North American (PNA) oscillation (Wallace and Gutzler, 1981; Barnston and Livezey, 1987). Warm (cold) ENSO events are associated with a positive (negative) phase of the PNA (e.g. Hamilton, 1988; Hoerling *et al*., 1997; Kumar and Hoerling, 1997; Lee *et al*., 2002). Even though Straus and Shukla (2000) and Shukla *et al*. (2000) found a difference between the typical PNA pattern and the mean anomaly pattern associated with ENSO events, in an ensemble of atmospheric general circulation model (AGCM) runs forced by prescribed SST (see Straus and Shukla (2000: Figure 11)), all these authors found that the Aleutian low is intensified and shifted toward the North American west coast during warm ENSO events in winter. The response during cold ENSO events is not strictly symmetrical and indicates a weakening of the Aleutian low's central pressure with little phase shift (e.g. Hoerling *et al*., 1997).

Over the North Atlantic and Europe, the dominant pattern of variability in SLPA is the North Atlantic oscillation (NAO), accounting for 35–40% of the seasonal variance and characterized by a see-saw between the Azores high and the Icelandic low (Rogers, 1984; Hurrell, 1995; Marshall *et al*., 2001; Slonosky and Yiou, 2002). Rogers (1984) found that the correlations between the NAO index (defined as the difference between December–February (DJF) SLPA at Ponta Delgada and Akureyri) and Darwin pressure at different lags never exceeded 0.2 over the 1900–83 period. The impact of ENSO on the North Atlantic domain is thus much weaker and less robust than in the PNA region (Fraedrich, 1990, 1993; Fraedrich and Muller, 1992; May and Bengtsson, 1998; Moron and Ward, 1998; Dong *et al*., 2000; Pozo-Vazquez *et al*., 2001). Nevertheless, the above studies showed that the mean SLPA pattern over the North Atlantic and Europe during warm (cold) ENSO events presents a generally negative (positive) SLPA over the central North Atlantic and a positive (negative) one north of 60 °N. This pattern is consistent with a weakening (strengthening) of the normal north–south SLP gradient across the North Atlantic and thus a negative (positive) phase of the NAO during the warm (cold) ENSO events (Rogers, 1984). Moreover, several numerical experiments with AGCMs forced by prescribed global SST indicate that the leading 'SST-forced' SLP mode over the NAE domain matches closely the NAO and is strongly related to ENSO even if the 'SST-forced' variance is quite low (e.g. Davies *et al*., 1997; Venzke *et al*., 1998; Feddersen, 2000; Cassou and Terray, 2001; Hannachi, 2001; Moron *et al*., 2001; Terray and Cassou, 2002; Sutton and Hodson, 2003). The detection of the impact of ENSO over the NAE sector is improved by separately analysing November–December and January–March (JFM) (Huang *et al*., 1998; Gouirand and Moron, 2000; Moron and Gouirand, 2003; Moron and Plaut, 2003).

Many of the diagnostic studies cited above have attempted to find the average extratropical effects through analysis of data spanning several ENSO cycles. Several studies (Hamilton, 1988; Rodo *et al*., 1997; Huang *et al*., 1998; Rocha, 1999; Gouirand and Moron, 2000; van Oldenborg *et al*., 2000; Moron and Plaut, 2003) emphasized the instability of the relationship between the ENSO and the North Atlantic atmospheric circulation in boreal winter and spring. In particular, Hamilton (1988: Figures 13–15), showing the Northern Hemisphere SLPA (in DJF) for the ENSO phases of 1925–26, 1957–58, and 1972–73, indicates very different patterns over the North Atlantic. The inter-event variability of the ENSO signal over the North Atlantic domain may be due to various factors, such as the strength and the inter-event variability of ENSO itself (e.g. Hamilton, 1988), the unpredictable internal atmospheric variability of the North Atlantic (e.g. Kumar and Hoerling, 1997) and the modulating influence of climatic modes independent of ENSO (e.g. Gershunov and Barnett, 1998; Moron and Plaut, 2003).

This paper examines the inter-event variability of the JFM SLPA over the North Atlantic domain during the 30 warmest and coldest ENSO events from 1874 to 1996. Section 2 presents the data and methods used. Mean SLPA patterns for the 30 warmest (coldest) ENSO events are computed. Then, Ward's clustering algorithm is applied to group warm (cold) ENSO events with similar SLPA patterns over the NAE sector. A three-cluster solution is chosen. The mean composites for SLPA on a larger domain encompassing the whole North Pacific sector are analysed for each cluster. Results are presented in Section 3. A summary (Section 4) closes the paper.

2. DATA AND METHODS

2.1. Data

The SLP data are on a 5° latitude by 5° longitude grid, cover the period 1874–1996, and have been used recently by Pozo-Vazquez *et al*. (2001) and Moron and Gouirand (2003). They were provided by T. Basnett of the UK Meteorological Office at Bracknell (Basnett and Livezey, 1997). The seasonal JFM mean is first computed from the monthly SLPA. Missing values are replaced by the seasonal mean. Then, SLPAs are computed for each grid point as departures from the long-term mean of the entire 1874–1996 period. Two domains are analysed: (i) the NAE sector (25–70 °N, 100 °W–50 °E) and (ii) a larger sector encompassing the North Pacific Ocean (hereafter NPAC–NAE) (25–70 °N, 120–50 °E). The cluster analysis is performed on the NAE domain, but the SLPAs are displayed on the NPAC–NAE sector to investigate the relationships between the North Atlantic and North Pacific areas.

Certain analyses described in Section 3 are repeated on a filtered SLPA data set from which the linear influence of the NAO has been removed. The NAO is the first empirical orthogonal function (EOF) of the NAE (Figure 1(a)) and NPAC–NAE (not shown) and accounts respectively for 40.2% and 24.8% of the seasonal JFM variance. This pattern also emerges as the leading mode of the whole Northern Hemisphere wintertime (December–March) SLPA (e.g. see Ambaum *et al*. (2001: Figure 1(a)). The correlation between time coefficients (spatial pattern) of EOF #1 of NAE and NPAC–NAE equals 0.97 (0.99). The low-frequency (LF) variability (frequency <0.1 cycles per year (cpy)) of the NAO represents 27% of the total variance (Figure 1(b)) and exhibits positive (negative) values, indicating a strengthening (weakening) of the zonal flow across the North Atlantic from 1900 to 1930, then after 1972, mainly during the late 1980s and the 1990s (from 1885 to 1900 and from 1935 to 1970, mainly the 1950s and 1960s) (e.g. Hurrell, 1995; Portis *et al*., 2001). The 'NAO-removed' SLPA fields are computed by multiplying the time coefficients of EOFs #2–122 (equal to the number of non-zero EOFs) with the associated spatial patterns (von Storch and Zwiers, 1998). In the following, the time coefficients of EOF #1 (Figure 1(b)) are used as a multivariate NAO index.

The 30 warm and cold ENSO events are based on the first EOF of the seasonal (October–March) SSTA in the tropical Pacific, already used in Moron and Gouirand (2003: Table I). This index is called TPAC hereafter. Note that considering the JFM seasonal mean instead of the October–March mean does not change the final results. The remaining 63 years are considered 'neutral' years.

2.2. Methods

Composites of SLPA are computed, based on the 30 warm (30 cold) ENSO events (Moron and Gouirand, 2003: Table I) to determine the typical SLPA response associated with warm (cold) events and each cluster. A Student's *t*-test (von Storch and Zwiers, 1998) is applied to find which anomalies are significantly different from the mean of the 'neutral' years at the two-tailed 0.1 level. Positive (negative) significant SLPAs are indicated by light (dark) shadings on the maps (Figures 2 and 4). The inter-event variability of the warm and cold ENSO events is studied through two methods. First, the difference of variance between warm (cold) ENSO events and 'neutral' years is computed (Smith *et al*., 1998), and a Fisher test is applied to test the results with the null hypothesis that the variances of both samples are equal. The significant area (at the two-tailed 0.1 level) is shaded in Figure 2(e) and (f). Second, the pattern correlation (p.c. hereafter) between the whole set of 123 years and the mean composite SLPA pattern (30 warm or 30 cold ENSO events) is computed (Figure 3(a) and (b)). The significance is derived using a permutation procedure; 500 samples of 30 years are extracted from the 63 'neutral' years and the p.c. is computed between the mean SLPA pattern and its 30 members. The level of significance is extracted from the ordered distribution of the 30×500 p.c. This cluster analysis is performed after composite analysis in order to classify the different patterns associated with the warm and cold ENSO events.

Cluster analysis is performed on the NAE SLPA fields for the 30 warm and cold ENSO events. Our goal here is to detect the individual SLPA patterns synchronous with warm and cold ENSO events that are most similar, and to group them together into one entity or cluster. In other words, our main goal is not to extract the 'true' clusters from the data, but to find an adequate subdivision of the SLPA patterns synchronous with

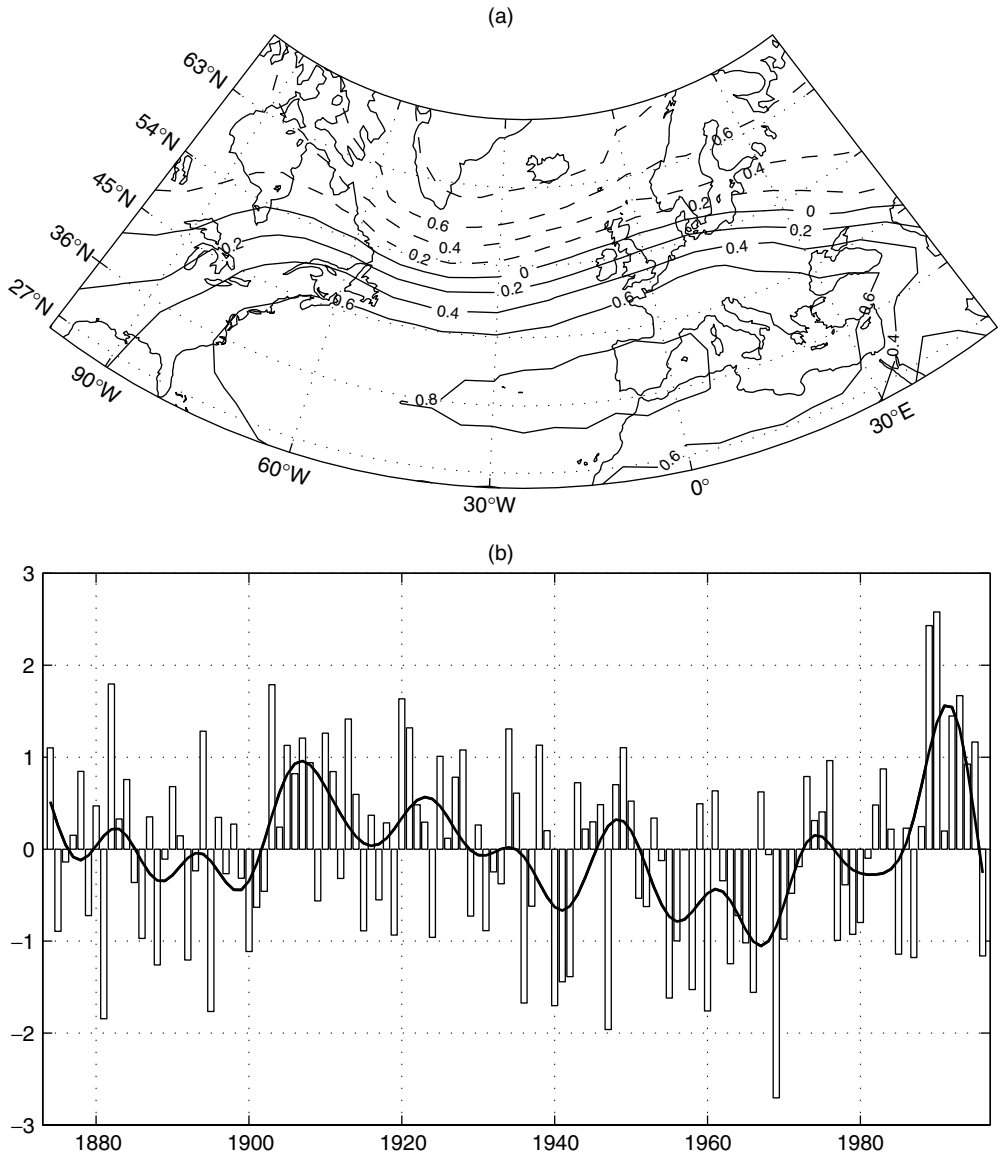

Figure 1. (a) Leading EOF of wintertime (January–March) SLPA (1874–1996). The contours express the correlations between the time coefficients of the EOF and the SLPA (from −0.8 to 0.8 with an interval of 0.2; negative loadings are dashed). (b) Standardized time coefficients (bars) and low-frequency variability (frequency <0.1 cpy) of the leading EOF. The low-frequency variability is estimated with a recursive Butterworth filter superimposed as a bold line

warm and cold ENSO events, in order to define several 'typical' patterns without sacrificing too much detail. The Euclidean distance is used to measure the dissimilarity between clusters (Fovell and Fovell, 1993; Gong and Richman, 1995). The range of Euclidean distance is from zero (for identical observations) to $+\infty$ (for observations with no relationships). The clusters are aggregated using Ward's method (Cheng and Wallace, 1993; Fovell and Fovell, 1993; Gong and Richman, 1995), which is designed to generate clusters so that mergers at each stage are found to minimize the within-groups sum of squares (Gong and Richman, 1995). The procedure used here is agglomerative, beginning with a set of individual observations, and then building up groups by a process of accumulation. The final outcome is a single cluster of 30 observations. A decision must be made as to when to halt the clustering. No technique is commonly accepted as a statistically justifiable

Table I. First row: surface locally significant (at the two-tailed 0.1 level) for the warm and cold ENSO samples in NAE SLPA according to Student's t-test (H0: mean of the sample equals the mean of neutral years). Second row: surface locally significant (at the two-sided 0.1 level) for the warm and cold ENSO samples in NAE SLPA (without the EOF #1) according to Student's t-test (H0: mean of the sample equals the mean of neutral years). For the first and second rows, the values in parentheses give the 'field significance' (i.e. the probability to find randomly a larger area locally significant at the two-tailed 0.1 level than the observed one) estimated with a Monte Carlo procedure (i.e. two samples of 30 and 63 other years are extracted randomly 500 times from the 123 years and the difference of their means is tested). Third row: mean score for EOF #1 time coefficients (see Figure 1(b)) for warm and cold ENSO samples and significance using Student's t-test (H0: mean of sample equals the mean of neutral years)

	Warm ENSO	Cold ENSO
NAE SLPA	20% (0.14)	15.9% (0.25)
NAE SLPA (−EOF #1)	28.4% (0.02)	8.2% (0.50)
NAO index	−0.19 (0.53)	+0.29 (0.10)

method (Fovell and Fovell, 1993; Gong and Richman, 1995). The choice retained here (three clusters) is a compromise between the small sample size and the interpretation of the SLPA pattern associated with each cluster. The internal homogeneity of each cluster is measured by the mean Euclidean distance between the centre of the cluster and each of its members. The observed value is compared with 500 samples randomly chosen in the 30 warm or cold ENSO years and having the same size as the observed cluster.

3. RESULTS

3.1. Stability of the observed SLPA pattern during warm and cold ENSO events

3.1.1. Mean SLPA pattern during the 30 warmest (coldest) ENSO events. Composites of SLPA over the NAE sector in JFM are shown for the 30 warm ENSO events (Figure 2(a)) and for the 30 cold ENSO events (Figure 2(b)). Composites are repeated with the 'NAO-removed' SLPA data set (see Section 2.2) and are shown for the 30 warm (Figure 2(c)) and 30 cold (Figure 2(d)) ENSO events. During warm ENSO events (Figure 2(a)), positive SLPAs are located over northeastern Canada and Greenland, whereas negative SLPAs stretch from the southeastern US coast and western North Atlantic to central and northern Europe. This pattern is associated with a weakening and/or a southward shift of the westerlies over the North Atlantic Ocean, even though the highest SLPAs are shifted westward with respect to the centres of action of the NAO (Giannini *et al*., 2001; Moron and Gouirand, 2003). The SLPA pattern is almost unchanged in the 'NAO-removed' SLPA data set (Figure 2(c)), and the area covered by significant anomalies at the two-tailed 0.1 level increases (Table I). This result suggests that the mean SLPA response during warm ENSO events is independent of the NAO, even though there is a weak preference for observing the negative phase of the NAO during warm ENSO events (Rogers 1984; Giannini *et al*., 2001; Moron and Gouirand, 2003). During cold ENSO events (Figure 2(b)), positive SLPAs are located from the southeastern US coast to western and central Europe and negative ones are located north of 55 °N. This SLPA pattern closely resembles the positive phase of the NAO (Figure 1(a)), with a strengthening of the Azores high and a deepening of the Icelandic low. Note also the strong decrease of the significant values at the two-tailed 0.1 level in the 'NAO-removed' SLPA data (Figure 1(d) and Table I) and the significant positive anomaly NAO index observed during the 30 coldest ENSO events (Table I). So, there is an asymmetry between the mean SLPA patterns associated with warm and cold ENSO events with the latter pattern projecting more strongly onto the NAO than the former.

3.1.2. Variability of the SLPA during the 30 warm (cold) ENSO events. Figure 2(e) (Figure 2(f)) shows the difference in standard deviation between the 30 warm (cold) ENSO events and neutral years. The SLPA is more variable during the 30 warm ENSO events than in neutral years over the central North Atlantic, across the main storm track (Figure 2(e)). The SLPA during the 30 cold ENSO events is never significantly greater

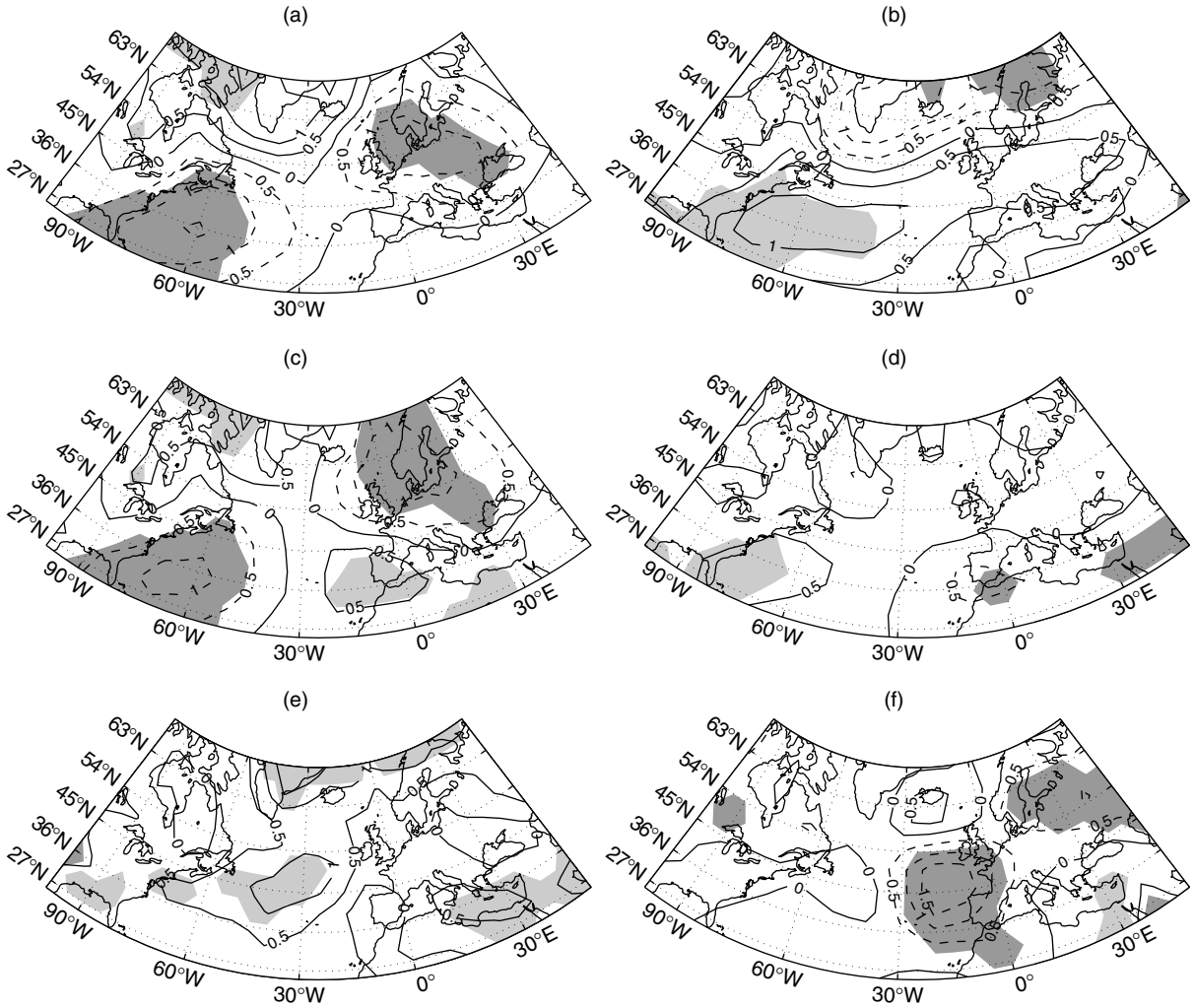

Figure 2. (a) Mean SLPA for the 30 warm ENSO events and (b) the 30 cold ENSO events in JFM. (c) Mean SLPA for the 30 warm ENSO events and (d) the 30 cold ENSO events in JFM when the linear influence of the NAO is removed. Units are hPa and the contour interval is 50 Pa. The positive (negative) significant SLPAs relative to the mean of the 'neutral' years at the 0.1 two-tailed level (using a Student's *t*-test) are shaded in light (dark) grey. (e) Difference of standard deviation between the 30 warm ENSO events and (f) 30 cold ENSO events on the one hand and the 'neutral' years on the other hand. Units are hPa. The positive (negative) significant differences at the 0.1 two-tailed level (using a Fisher test) are shaded in light (dark) grey

than that of the neutral years (Figure 2(f)). The variance of the cold ENSO sample is then lower than during the neutral years in the eastern North Atlantic (Figure 2(f)). Both figures show that SLPAs related to cold ENSO events are more stable than those associated with warm ENSO events, consistent with the results of Hannachi (2001) and Pozo-Vazquez *et al.* (2001).

Figure 3(a) (Figure 3(b)) shows the p.c. between the mean SLPA pattern for the 30 warm (cold) ENSO events displayed in Figure 2(a) (Figure 2(b)) and the 123 individual JFM seasons. The top one-tailed 0.1 random p.c. is 0.58 for the NAE sector, displayed as a straight line in Figure 3(a) and (b). Only seven warm ENSO events (i.e. 1915, 1919, 1931, 1941, 1958, 1966, 1970) have a significant p.c. with the mean SLPA of 30 warm ENSO events. Note that none of the 500 30-year random samples extracted from the neutral years have more than five significant p.c. with its mean SLPA composite. A few neutral years also have a significant p.c. with the mean SLPA pattern, mainly before 1905 and around 1960 (Figure 3(a)), meaning that the mean

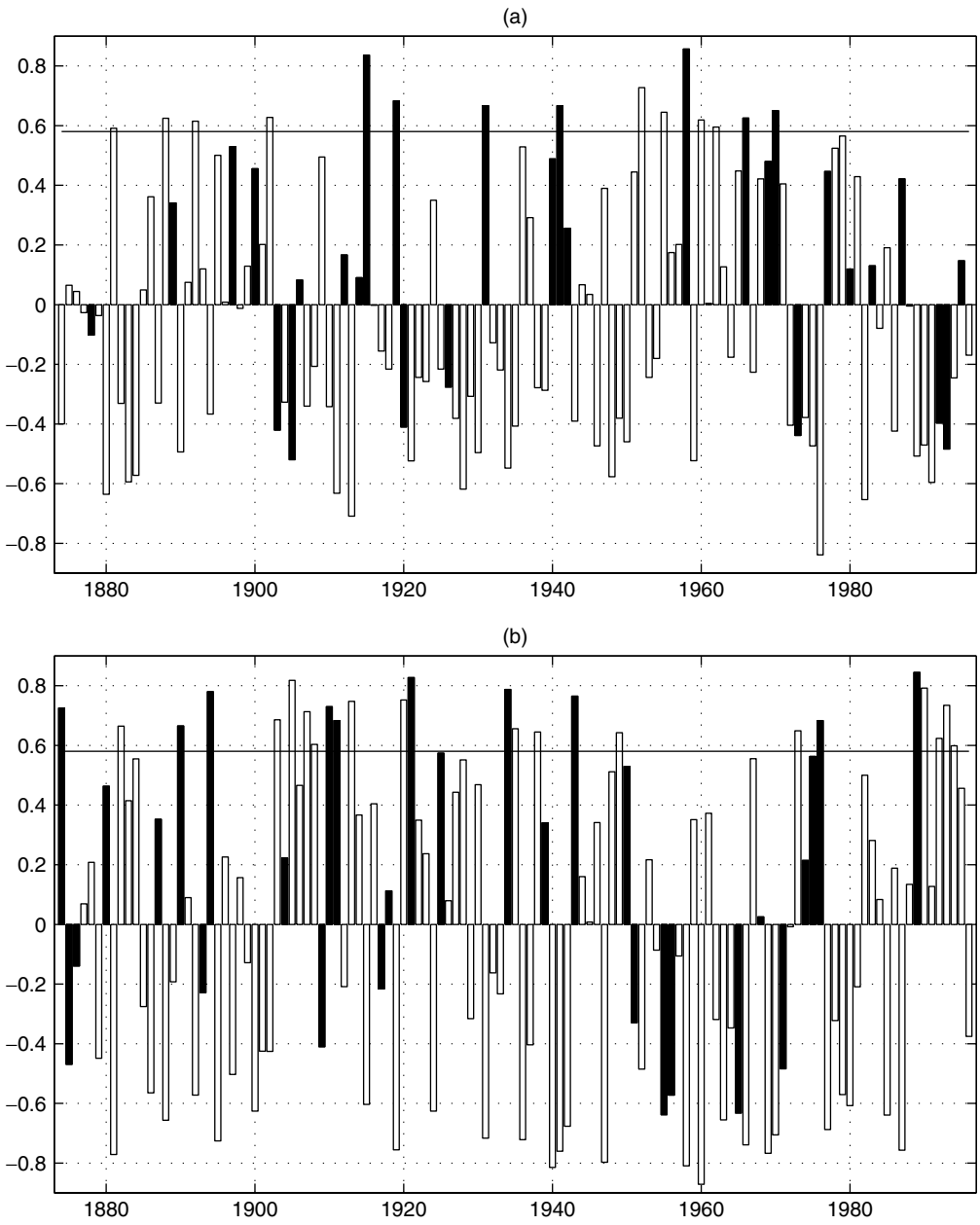

Figure 3. The p.c. between each SLPA and the mean SLPA pattern of (a) the 30 warm ENSO events and (b) the 30 cold ENSO events in JFM. The warm (a) and cold (b) ENSO events are identified as black bars. The horizontal line is the one-tailed 0.1 level of significance derived from a permutation Monte Carlo procedure (see text)

SLPA pattern associated with the warm ENSO (Figure 2(a)) events may appear without any strong SSTA in the tropical Pacific. The highest p.c. of the 30 warm ENSO years is clustered in time between 1930 and 1970, when the North Atlantic basinwide westerlies are anomalously slow (Deser and Blackmon, 1993; Kushnir, 1994; Marshall *et al*., 2001; Portis *et al*., 2001). The warm ENSO events during the 1900s, 1920s and then 1990s make the SLPA patterns deviate relative to the mean one (Figure 3(a)). Ten cold ENSO events (1874, 1890, 1894, 1910, 1911, 1921, 1934, 1943, 1976, 1989) have a significant p.c. with the mean SLPA pattern displayed in Figure 1(b) (see Figure 3(b)). Such an SLPA pattern also occurs during neutral years, mainly

in 1900–20, and then during the 1990s (Figure 3(b)). The six consecutive cold ENSO events from 1951 to 1971 have a zero or negative p.c. (Figure 3(b)), but the p.c. for the other years during these decades is also usually negative. The possible influence of multi-decadal variability of the North Atlantic SLPA is further investigated in Section 3.3.

3.2. SLPA patterns observed by cluster analysis

The previous section reveals that the mean SLPA patterns for 30 warm (cold) ENSO events (Figure 2(a) and (b)) is an average of various SLPA signals, mainly for warm ENSO events. Then, a cluster analysis is applied on the SLPAs of the NAE sector to classify the SLPA patterns associated with warm (cold) ENSO signals into three distinct groups. The evolution from two to four clusters is presented in Tables II and III. Three clusters have been kept for each case (warm and cold ENSO events). Cluster analysis is done over the NAE sector, but composites of SLPA (Figure 4) are displayed on a larger area between 120 °E and 50 °E to see the possible relationships between North Atlantic and North Pacific.

The three clusters (Table II) of warm ENSO events during JFM show highly significant SLPAs over the NAE sector. The first (Figure 4(a)) and third (Figure 4(c)) clusters have a reversed SLPA pattern. In the first cluster (Figure 4(a)), positive SLPAs are located over the North Atlantic, from eastern Canada to northern Europe, and negative ones stretch from the southeastern US coast to southern and central Europe. This pattern is strongly correlated (p.c. = 0.71 for the NAE sector) with the mean SLPA pattern shown in Figure 2(a) (Table II), and suggests a weakening and/or a southward shift of the westerlies in the central North Atlantic. This pattern is consistent with a negative NAO phase (Table IV) and is also similar to the negative phase of the so-called Arctic Oscillation (AO) (Thompson and Wallace, 1998; Wallace and Thompson, 2002), since Aleutian SLPAs are in-phase (out-of-phase) with Azores (Icelandic) ones (refer to Thompson and Wallace (1998: Figure 1)). In the third cluster (Figure 4(c)), on the contrary, positive SLPAs are located south of 55 °N between Newfoundland and Europe, and negative ones stretch from Greenland to northern Europe. This pattern is thus consistent with a positive NAO phase (Table IV). The second cluster (Figure 4(b)) presents only one centre of significant negative SLPA over the central North Atlantic Ocean. This cluster is the least

Table II. Cluster analysis results for the 30 warm ENSO events. The last column lists the 30 warm ENSO years with the 1–10th, 11–20th and 21–30th warmest years indicated in italic, bold, and normal font respectively. 'p.c.' is the correlation between the mean SLPA pattern of each cluster (Figure 4(a)–(c)) and the mean SLPA pattern of 30 warm ENSO events (Figure 2(a)). *d* is the mean Euclidian distance between the warm ENSO events of each cluster and the centroid of the cluster. Asterisks show significant values according to a Monte Carlo simulation at the 0.1 level. 'niño 3′ indicates the mean SST anomaly for the Niño3 box (5 °N–5 °S, 180–90 °W) for each cluster. The mean SSTA of 'niño 3′ for the 30 warm ENSO events is +1.05 °C. Asterisks indicate significant SSTAs (at the two-tailed 0.1 threshold) relative to the mean of the 30 warm ENSO events

Two clusters	Three clusters	Four clusters	Warm ENSO years
p.c. = 0.71 $d = 3.3^*$ niño3 = +1.0 °C			***1897*** ***1900*** **1915** ***1919*** ***1931*** 1940 ***1941*** **1942** **1958** **1966** 1969 1970 1980 **1987**
		p.c. = 0.14 $d = 2.5^*$ niño3 = +0.8 °C	1912 **1926** 1977
	p.c. = 0 $d = 3.8$ niño3 = $+0.8\,°C^*$		
p.c. = −0.25 $d = 4.4$ niño3 = +1.0 °C		p.c. = −0.09 $d = 3.8$ niño3 = +0.8 °C	**1903** 1914 **1995**
	p.c. = −0.3 $d = 3.6^*$ niño3 = +1.2 °C		***1878*** ***1889*** 1905 **1906** 1920 ***1973*** ***1983*** **1988** ***1992*** 1993

Table III. Cluster analysis results for the 30 cold ENSO events. The last column lists the 30 cold ENSO years with the 1–10th, 11–20th and 21–30th coldest years indicated in italic, bold, and normal font respectively. 'p.c.' is the correlation between the mean SLPA pattern of each cluster (Figure 4(a)–(c)) and the mean SLPA pattern of 30 cold ENSO events (Figure 2(b)). *d* is the mean Euclidian distance between the cold ENSO events of each cluster and the centroid of the cluster. Asterisks show significant values according to a Monte Carlo simulation at the 0.1 level. 'niño 3' indicates the mean SST anomaly for the Niño3 box (5 °N–5 °S, 180–90 °W) for each cluster. The mean SSTA of 'niño 3' for the 30 cold ENSO events is −0.88 °C. Asterisks indicate significant SSTAs (at the two-tailed 0.1 threshold) relative to the mean of the 30 cold ENSO events

Two classes	Three classes	Four classes	Cold ENSO years
	p.c. = 0.9 d = 2.9* niño3 = −1.0 °C		**1890** ***1894*** ***1910*** **1911** 1921 **1925** 1934 **1943** **1950** ***1989***
p.c. = 0.9 d = 3.3 niño3 = −0.9 °C	p.c. = 0.7 d = 3.3 niño3 = −0.8 °C	p.c. = 0.62 d = 2.5* niño3 = −0.7 °C	***1874*** 1880 **1887** **1918** 1975
		p.c. = 0.41 d = 2.5 niño3 = −1.0 °C	1904 ***1974*** ***1976***
p.c. = −0.7 d = 3.2* niño3 = −0.8 °C			**1875** **1876** ***1893*** **1909** ***1917*** 1939 1951 1955 ***1956*** 1965 1968 ***1971***

homogeneous (Table II). Over the North Pacific, the typical signal of warm ENSO events, characterized by a deepening and a southeastward shift of the Aleutian low (i.e. Kumar and Hoerling, 1997, 1998; Diaz *et al*., 2001; Pozo-Vazquez *et al*., 2001) is stable for the three clusters, even though the strongest SLPAs are observed in the first cluster (Figure 4(a)). A nearly identical response over the North Pacific area (first and third clusters) is associated with an almost reversed response over the North Atlantic (p.c. between the first and third cluster of −0.8 for the NAE sector). Note that the years included in each cluster seem to be concentrated in certain multi-decadal periods; it is particularly clear for the first cluster, which contains the eight consecutive warm ENSO events between 1931 and 1970 (Table II). This apparent concentration suggests a possible contamination of these patterns by the multi-decadal variability of the North Atlantic SLPA (Figure 1(b)). This question is investigated further in Section 3.3.

SLPA composites (Figure 4(d)–(f)) for the three clusters of the 30 cold ENSO events (Table III) were computed. For the three clusters, the SLPA response over the NAE sector is relatively high. The SLPA pattern is highly similar in cluster #1 (Figure 4(d)) and cluster #2 (Figure 4(e)), with weaker amplitude in the latter. Positive (negative) SLPAs are located over the North Atlantic southward (northward) of 55 °N in cluster #1, and southward of 45 °N and over Europe (between Ellesmere Island and Iceland) in cluster #2 (Figure 4(d) and (e)). Both patterns are consistent with a positive phase of the NAO (Table IV), and the first one projects strongly onto the positive phase of the AO (Thompson and Wallace, 1998; Wallace and Thompson, 2002). The years included in these two clusters are concentrated before 1940, then from 1974 (Table III). The pattern of cluster #3 (Figure 4(f)) is reversed relative to those of the first and second clusters, with positive SLPAs over Greenland and negative SLPAs over southern Europe and the Mediterranean area. The NAO index is now significantly negative (Table IV). Over the North Pacific, SLPAs have the same sign in the three clusters (Figure 4(d)–(f)). The positive SLPAs between 2 and 3 hPa around 180 °W and 45–55 °N are associated with a weakening of the Aleutian low (Diaz *et al*., 2001; Pozo-Vazquez *et al*., 2001), without a clear shift.

When composites are computed with the 'NAO-removed' data set (not shown), the area, locally significant at the two-tailed 0.1 level, decreases strongly for all clusters except for the second one of the warm ENSO events sample (Table IV). In particular, the 'field significance' of the first (all) cluster of the warm (cold)

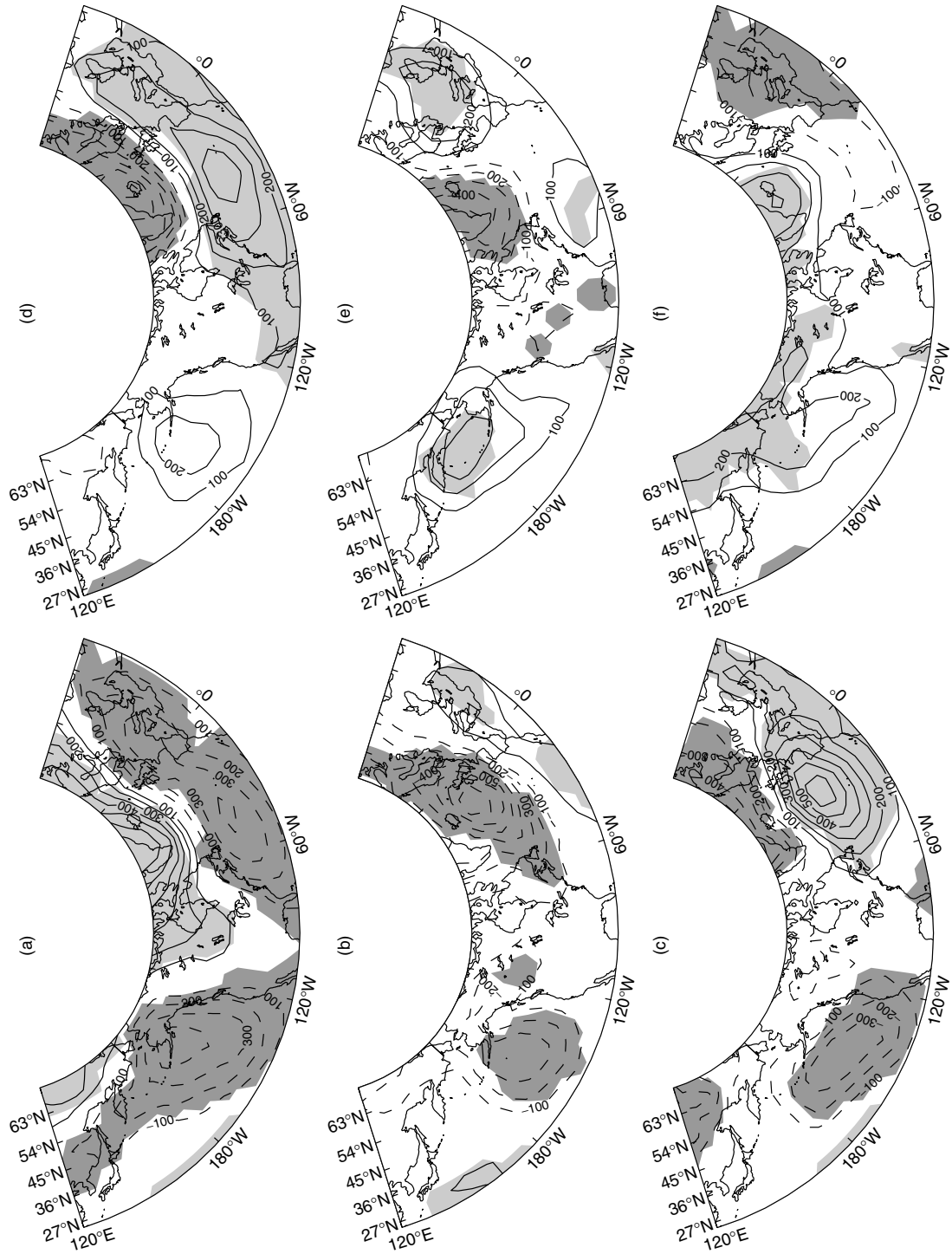

Figure 4. North Atlantic SLPA clusters constructed using Ward's hierarchical method for the 30 warm ENSO events (a, b, c) and the 30 cold ENSO events (d, e, f). The cluster analysis is performed on the NAE sector (25–70 °N, 100 °W–50 °E). Each map is the arithmetic average of North Pacific and North Atlantic SLPAs (relative to the long-term mean) belonging to that cluster. Units are pascals and the contour interval is 100 Pa. The clusters are ranked according to their p.c. (on the NAE domain only) with the mean SLPA pattern shown in Figure 2(a) and (b). The positive (negative) significant SLPAs, at the two-tailed 0.1 level and relative to the mean of the 'neutral', are shaded in light (dark) grey

Table IV. Second column: surface locally significant (at the two-tailed 0.1 level) for the warm and cold ENSO samples in NAE SLPA according to a Student's t-test (H0: mean of the sample equals the mean of neutral years). Third column: surface locally significant (at the two-tailed 0.1 level) for the warm and cold ENSO samples in NAE SLPA (without the EOF #1) according to a Student's t-test (H0: mean of the sample equals the mean of neutral years). For the second and third columns the values in parentheses give the 'field significance' (i.e. the probability to find randomly a larger area locally significant at the two-tailed 0.1 level than the observed one) estimated with a Monte Carlo procedure (i.e. two samples of n ($n = 6$, 8, 10, 12 or 14 years, depending on the size of the cluster tested) and 63 other years are extracted randomly 500 times from the 123 years and the difference of their means is tested). Fourth column: mean anomaly (and its associated two-tailed level of significance according to a Student's t-test with the null hypothesis that the mean of the sample equals the mean of the neutral years) of the NAO index (equals time score of the first EOF of NAE SLPA)

	NAE SLPA	NAE SLPA-EOF #1	NAO index
Warm ENSO–cluster #1	69.9% (0)	16.0% (0.21)	−1.2 (<0.01)
Warm ENSO–cluster #2	29.1% (0.09)	33.8% (0.01)	+0.4 (0.27)
Warm ENSO–cluster #3	52.7% (0.002)	26.4% (0.04)	+0.9 (<0.01)
Cold ENSO–cluster #1	72.1% (0)	17.7% (0.15)	+1.2 (<0.01)
Cold ENSO–cluster #2	24.7% (0.10)	14.7% (0.22)	+0.6 (0.09)
Cold ENSO–cluster #3	27.5% (0.06)	11.0% (0.38)	−0.5 (0.06)

ENSO events sample is now well above the one-sided 0.1 level (Table IV). This suggests that the main 'typical' SLPA patterns associated with warm and cold ENSO events project themselves, more or less, onto the NAO pattern. It is particularly clear for the cold ENSO events, with a strong preference (clusters #1 and #2 here) for a positive NAO phase. The warm ENSO events are less systematically associated with a negative phase of the NAO.

3.3. Influence of the multi-decadal variability in the NAE area

The previous sections show a large inter-event variability of the North Atlantic SLPA response to ENSO events, mainly during the warm phase. The fact that years included in one cluster seem concentrated in time raises the possibility that their associated SLPA patterns are a better indicator of the multi-decadal variability of the NAE atmosphere rather than any significant relationship with a warm ENSO event (Giannini *et al.*, 2001). To see the influence of the multi-decadal variability, the seasonal JFM SLPA fields were filtered with a recursive Butterworth filter with a cut-off at 0.1 cpy. The high-pass (frequency >0.1 cpy) and low-pass (frequency <0.1 cpy) components of the SLPA data set, NAO and TPAC indices are called HF and LF hereafter respectively. The composites of the HF SLPA were computed (not shown) for the three clusters of the warm and cold ENSO events. The six HF SLPA patterns are highly correlated with those displayed in Figure 4 (p.c. >0.9). Table V indicates the area locally significant at the two-tailed 0.1 level in the clusters computed with the HF SLPA data set. Even though the areas locally significant are reduced relative to that obtained with the full data set (compare first columns of Tables IV and V), the SLPA patterns of each cluster usually remain 'field significant' at the one-tailed 0.1 level, mainly for the warm ENSO events. For the cold ENSO events, the SLPAs associated with the second and third clusters are strongly reduced in the HF data set. This reduction suggests that the SLPA pattern of the second (Figure 4(f)) and mainly the third (Figure 4(e)) clusters is almost entirely accounted for by the fact that years are clustered into a particular multi-decadal phase of the NAE SLPA. Thus, this SLPA pattern may not represent a real relationship between the cold ENSO event and the North Atlantic SLPA.

The possible multi-decadal modulation of the warm (cold) ENSO event relationship with the NAE atmospheric domain is investigated further with running correlations and composites (Figure 5). We focus here on the NAO index, defined in Section 2.1 (Figure 1), since at least five clusters out of six could be well identified as negative or positive phases of the NAO. Figure 5(a) displays the correlations between the HF TPAC and NAO indices on sliding windows of 11, 21 and 31 years. The inter-decadal swings in the relationship are common to all sliding window widths; in particular, there is an abrupt shift to negative

Table V. Second column: area significant (at the two-tailed 0.1 level) for the warm and cold ENSO samples in HF NAE SLPA according to a Student's t-test (H0: mean of the sample equals the mean of neutral years). The values in parentheses give the 'field significance' (i.e. the probability to find randomly a larger area locally significant at the two-tailed 0.1 level than the observed one) estimated with a Monte Carlo procedure, i.e. two samples of n ($n = 6$, 8, 10, 12 or 14 years, depending on the size of the cluster which is tested) and 63 other years are extracted randomly 500 times from the 123 years and the difference of their means is tested. Third column: mean anomaly (and its associated two-sided level of significance according to a Student's t-test with the null hypothesis that the mean of the sample equals the mean of the neutral years) of the HF NAO index (equals time score of the first EOF of NAE SLPA)

	HF NAE SLPA	HF NAO index
Warm ENSO–cluster #1	59.1% (0)	−1.00 (<0.01)
Warm ENSO–cluster #2	27.4% (0.07)	+0.17 (0.66)
Warm ENSO–cluster #3	39.8% (0.02)	+0.52 (0.11)
Cold ENSO–cluster #1	67.7% (0)	+1.04 (<0.01)
Cold ENSO–cluster #2	12.3% (0.29)	+0.41 (0.25)
Cold ENSO–cluster #3	9.4% (0.42)	−0.37 (0.27)

correlations from around 1925 to 1950. The standard deviations of running correlations between the observed HF time series of TPAC and NAO for the 11 years, 21 years and 31 years are 0.271, 0.195 and 0.157 respectively and thus are not distinguishable from those expected from noise when the correlation between both time series equals −0.21 (see Gershunov *et al.* (2001: Table I)). In other words, the decadal modulation shown in Figure 5(a) could be due solely to stochastic processes. An alternative method for evaluating the non-stationarity of the relationship between ENSO and NAO is to compute the composite on sliding windows (Figure 5(b)). The mean HF NAO anomaly corresponding to warm (cold) ENSO years in sliding 21 year windows is computed and tested relative to the neutral years included in these windows. This figure indicates clearly that the HF ENSO–NAO relationship, even around 1925–50, when the correlations between both indices equal −0.6 to −0.7 on the 21 year window, is not strictly symmetrical (except around 1930 and 1940, when warm (cold) ENSO events lead to almost equal negative (positive) NAO anomalies). Warm ENSO events between 1925 and 1970 (which are grouped together in the first cluster) are associated consistently with a negative NAO phase, as already observed in Sections 3.2. The shift toward negative values is particularly abrupt when the warm ENSO event of 1920 is replaced by that of 1940. In contrast, the consecutive cold ENSO events reveal a significant (at the 0.1 one-tailed level) positive NAO phase around 1890, then around 1925–40, then after 1970 (Figure 5(b)). The first decrease of the NAO anomalies during cold ENSO events, occurring near 1905–10 (Figure 5(b)), is mainly due to the very strong negative HF NAO in 1909 (equal to −1.6, which is the highest absolute anomaly during the 30 cold ENSO years with the one of 1989).

These results suggest that the ENSO–NAO (and more generally ENSO–NAE atmospheric circulation) relationships could be modulated by an LF process. The next step is to find a plausible physical origin for such a modulation. The strong relationship between warm ENSO events and the negative NAO phase during 1930–70 may hardly be explained by the intensity of ENSO events itself, since warm ENSO events are weak (except in 1941) during that period. Even if the NAO is usually viewed as an internal atmospheric mode, several numerical studies involving AGCMs forced by prescribed observed SSTs (e.g. Cassou and Terray, 2001; Terray and Cassou, 2002; Sutton and Hodson, 2003) or by idealized SST patterns (Peng *et al.*, 2002) indicated that North Atlantic SSTs are able to force the NAO on interdecadal and interannual time scales. In particular, Terray and Cassou (2002) showed that positive tropical North Atlantic SSTAs are able to force a negative phase of the NAO. The forcing of cold SSTAs onto a positive phase of the NAO is weaker (Terray and Cassou, 2002). Such asymmetry is also indicated by Peng *et al.* (2002). It is well known that the north tropical Atlantic warms 3–6 months after the eastern and central equatorial Pacific (e.g. Curtis and Hastenrath, 1995; Enfield and Mayer, 1997; Moron and Ward 1998), but it could be hypothesized that the LF variability of the tropical North Atlantic is independent of warm (cold) ENSO events. So, multi-decadal variability of the tropical North Atlantic could modulate the ENSO–NAE atmosphere relationship. A tropical North Atlantic

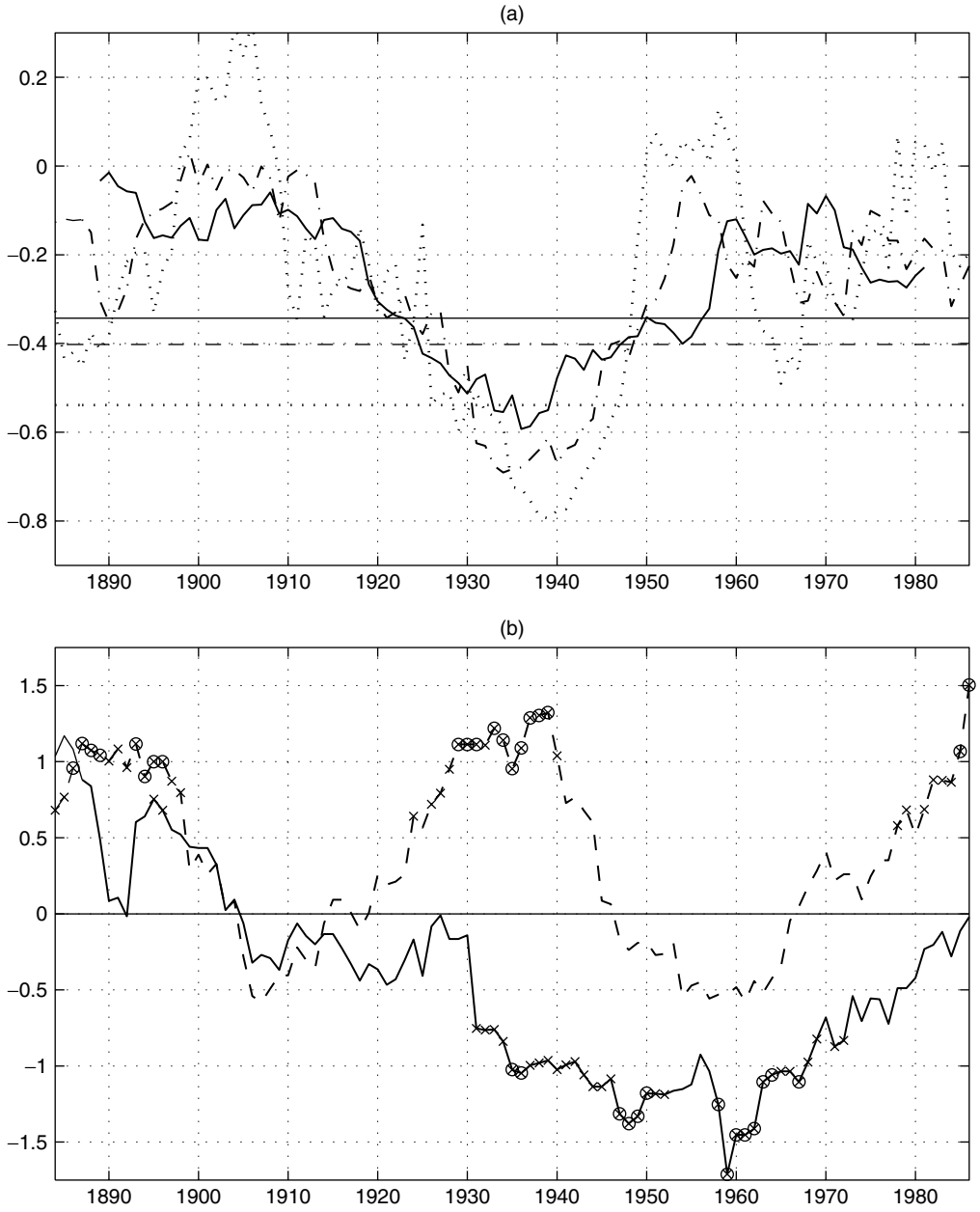

Figure 5. (a) Running correlations between the HF TPAC and NAO indices on 11-year (dotted line), 21-year (dotted–dashed line) and 31-year (full line) sliding windows. The straight lines indicate the one-tailed 0.05 level of significance estimated with a Monte Carlo procedure (i.e. two random time series having the same spectral power as the HF TPAC and NAO are correlated 500 times on sliding windows and the resultant correlations are ordered); (b) running composite of the HF NAO on sliding 21-year windows for warm (cold) ENSO in full (dashed) line. The anomalies in each window are computed relative to the neutral years included in this window. The cross (circle and cross) indicates significant anomalies according to a Student's *t*-test at the one-tailed 0.1 (0.05) level (H0: the mean of high-pass NAO during warm or cold ENSO events equals the mean of high-pass neutral years; H1: the mean of high-pass NAO during warm (cold) ENSO events is lower (higher) than the mean of high-pass neutral years)

index (TNA) is computed by averaging SSTAs in the box 20–80 °W and 10–20 °N in December. It is shown in Figure 6(a) with its LF variability superimposed as a thick dashed line. The LF values of the December TNA are considered since the JFM values could force the NAO but they also contain the forcing from the NAO

(e.g. Zorita *et al*., 1992; Lau, 1997; Lau and Nath, 2001). Inter-decadal and multi-decadal variance explains a larger fraction (60%) than for the JFM NAO index, but the swings between both indices are clearly out of phase (compare Figures 1(b) and 6). Table VI suggests that, on the one hand, the combination of warm LF TNA in December and warm ENSO events and, on the other hand, cold LF TNA in December and cold ENSO events are moderately related to negative and positive phases of the HF NAO in JFM respectively. The two other combinations (i.e. cold LF TNA + warm ENSO and warm LF TNA + cold ENSO) lead to the same HF NAO anomaly but with a reduced amplitude (Table VI). Note that neutral years are associated with very weak NAO and HF NAO anomalies. In other words, the LF TNA phase in December seems unable to force, alone, significant anomalies of the HF NAO in JFM.

4. CONCLUSIONS

We have investigated the instability of the relationship between warm (cold) ENSO events and the atmospheric surface anomalies over the NAE sector in JFM (1874–1996). The JFM season is used since it appears to be better suited than DJF for the study of the impacts of warm (cold) ENSO events over this sector (Huang *et al*., 1998; Gouirand and Moron 2000; Moron and Gouirand, 2003; Moron and Plaut, 2003). Pattern correlation and cluster analysis are used to study the variability of the weak relationship between warm (cold) ENSO events and the NAE atmospheric response.

The mean SLPA pattern for the cold ENSO events is stable during the entire period (Hannachi, 2001; Pozo-Vazquez *et al*., 2001). There is a robust increase in the usual north–south SLP gradient across the North Atlantic. This SLP pattern is associated with stronger than usual and northward-shifted westerlies, i.e.

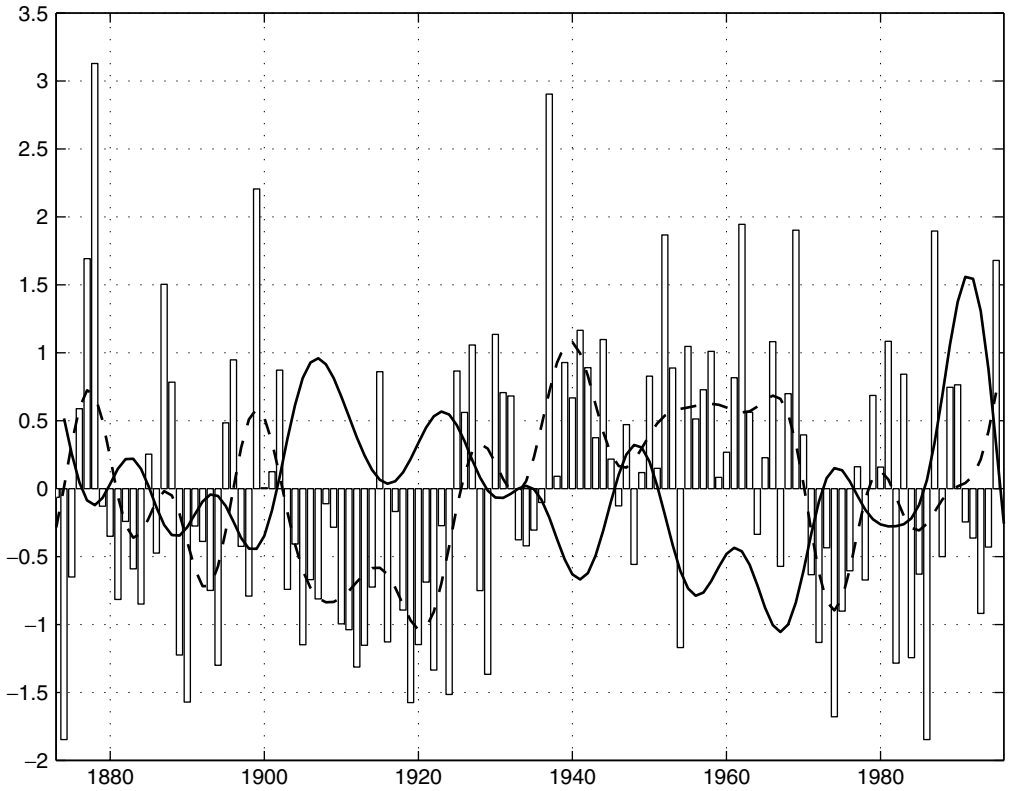

Figure 6. Tropical North Atlantic SSTAs in December (1873–1995) in bars and LF (i.e. frequency <0.1 cpy) component superimposed as a dashed black line. The LF component of the JFM NAO (see Figure 1(b)) is superimposed as a full black line. The units are standard deviations

Table VI. Mean anomaly of NAO (column 2) and mean anomaly of HF NAO index (column 3) for various combinations involving warm and cold ENSO and December LF tropical North Atlantic SSTAs. Each time series (NAO and HF NAO) is first standardized to zero mean and unit variance. For the first four lines, the values in parentheses give the two-sided level of significance according to a Student's t-test (H0: the mean of the warm and cold ENSO samples equals the mean of neutral years included in the same LF TNAT phase)

	NAO index	HF NAO index
Warm ENSO + warm LF TNAT	−0.48 (0.27)	−0.38 (0.21)
Warm ENSO + cold LF TNAT	+0.10 (0.90)	−0.14 (0.92)
Cold ENSO + warm LF TNAT	−0.27 (0.60)	+0.16 (0.71)
Cold ENSO + cold LF TNAT	+0.62 (0.07)	+0.39 (0.09)
Neutral + warm LF TNAT	−0.12	+0.03
Neutral + cold LF TNAT	+0.06	−0.11
Warm ENSO	−0.19	−0.26
Cold ENSO	+0.29	+0.31

is a positive phase of the NAO. A slight difference among the 30 cold ENSO events is associated with the presence or absence of a positive SLPA in central and northern Europe (identified here by the second cluster; Figure 4(e)). This robust response almost vanishes during the 1950s and 1960s, when the basinwide westerlies are anomalously slow (Deser and Blackmon, 1993; Kushnir 1994; Hurrel and van Loon, 1997; Shabbar *et al*., 1997; Marshall *et al*., 2001; Slonosky and Yiou, 2002). During that period, the SLPAs associated with cold ENSO events display a reversed SLPA pattern across the North Atlantic (i.e. positive (negative) SLPA north (south) of 50 °N), but these SLPAs are not significant when the multi-decadal variability of the North Atlantic SLPA is removed.

There is considerable variability around the mean SLPA composite associated with the warm ENSO events (Hannachi, 2001; Pozo-Vazquez *et al*., 2001). Two homogeneous and almost reversed SLPA patterns emerge in the NAE sector. The first one is the most frequent and then appears, more weakly and slightly distorted, in the mean SLPA composite of the 30 warm ENSO events (Figure 2(a)). This pattern is characterized by positive (negative) SLPAs north (south) of 50 °N, i.e. a negative phase of the NAO. It particularly appears from 1930 to 1970, when the basinwide westerlies are weakened relative to the long-term mean (Deser and Blackmon, 1993; Kushnir, 1994; Hurrell and van Loon, 1997; Shabbar *et al*., 1997; Marshall *et al*., 2001) and when the 'passive' mode of Raible *et al*. (2001) dominates. Nevertheless, these SLPAs (and the negative phase of the NAO) remain statistically significant even when the LF variability is removed. The second homogeneous SLPA pattern is almost reversed over the NAE sector and is associated with a northward shift of the westerlies over the central and eastern North Atlantic. This pattern occurs mainly during the beginning and the end of the 20th century, when the basinwide westerlies are strengthened and when the 'active' regional mode of Raible *et al*. (2001) dominates.

The inter-event variability of the ENSO–NAE atmosphere relationship could be influenced by a myriad of factors. It seems that the strength of warm and cold ENSO events is not the dominant factor. Firstly, the strongest cold and warm ENSO events are not systematically grouped into the most typical cluster (i.e. cluster #1). Secondly, the most consistent SLPA pattern during the warm ENSO events is mainly observed between 1930 and 1970, i.e. when these events are rather weak. Nevertheless, the least homogeneous cluster for the warm ENSO events (i.e. cluster #2) is associated with the lowest SSTA in Niño3. Note that an SSTA index located over the far western Pacific and Indonesian region (130–150 °E; 10 °S–10 °N), which is considered by Hamilton (1988) as a possible modulator of the warm (cold) ENSO events effect over the Northern Hemisphere circulation, does not also act as a change of the standard warm (cold) ENSO teleconnection pattern over the NAE sector (not shown). It is shown here that the north tropical Atlantic SSTA could exert a multi-decadal modulating effect on the ENSO–NAE atmosphere relationship. Several numerical studies (e.g. Terray and Cassou, 2002; Sutton and Hodson, 2003) indicate that warm TNA SSTAs are able to force (mainly at decadal and longer time scales) a negative phase of the NAO. So, the typical warm ENSO teleconnection pattern on the NAE sector (equal to a negative phase of the NAO) could then be particularly favoured during the warm

phase of the TNA, independently of the strength of the warm ENSO itself. The association between the cold TNA phase and the positive phase of the NAO during cold ENSO events is less clear, even if this relationship vanishes in the 1950s–60s when the TNA is anomalously warm (Figure 6). In the same order of ideas, the cold period around 1910–20 (Figure 6) is not systematically associated with a significant positive phase of the NAO during cold ENSO events (Figure 3(b) and Table III). It must be stressed here that the forcing of the cold TNA upon the positive phase of the NAO is weaker than the reverse one (Terray and Cassou, 2002). The reality and the causes of the second pattern associated with the warm ENSO patterns (identified here as cluster #3) also remain to be understood. We must remember here that these years, including very strong events (such as JFM 1983), could integrate a forcing other than a warm (cold) ENSO. These forcings (such as major volcanic tropical eruptions; Robock, 2000) could induce a different (and stronger) response than a warm ENSO.

Several factors other than the TNA, not analysed here, could exert a modulating influence on the ENSO–NAE atmosphere teleconnection, e.g. the unpredictable internal noise of the extratropical atmosphere or the teleconnection between North Pacific and North Atlantic area (Honda *et al*., 2001a,b; Raible *et al*., 2001). Nevertheless, our results suggest that any evaluation of the skill of AGCMs forced by prescribed SSTs (Venzke *et al*., 1998; Cassou and Terray, 2001; Hannachi, 2001; Terray and Cassou, 2002; Sutton and Hodson, 2003) should consider precisely the period taken into account, since the observed teleconnection pattern is variable over the North Atlantic area. Also, the results confirm the greater stability (and thus the better predictability) of the JFM SLPAs over the NAE sector that are associated with cold ENSO events rather than those related to warm ones.

ACKNOWLEDGEMENTS

We greatly appreciated the careful reading by Alessandra Giannini of the revised version of this paper.

REFERENCES

Ambaum MHP, Hoskins BJ, Stephenson DB. 2001. Arctic oscillation or North Atlantic oscillation? *Journal of Climate* **14**: 3495–3507.

Barnston AG, Livezey RE. 1987. Classification, seasonality and persistence of low-frequency atmospheric circulation patterns. *Monthly Weather Review* **115**: 1083–1121.

Basnett TA, Livezey RE. 1997. Development of the global mean sea level pressure data set GMSLP2. Climatic Research Technical note no. 79, Hadley Centre, Meteorological Office, Bracknell, UK.

Cassou C, Terray L. 2001. Oceanic forcing of the wintertime low-frequency atmospheric variability in the North Atlantic European sector: a study with the ARPEGE model. *Journal of Climate* **14**: 4266–4291.

Cheng X, Wallace JM. 1993. Cluster analysis of the Northern Hemisphere wintertime 500 hPa height field: spatial patterns. *Journal of the Atmospheric Sciences* **50**: 2674–2696.

Curtis S, Hastenrath S. 1995. The forcing of the sea surface temperature evolution in the tropical Atlantic during Pacific warm events. *Journal of Geophysical Research* **100**: 15 835–15 847.

Davies JR, Rowell DP, Folland CK. 1997. North Atlantic and European seasonal predictability using an ensemble of multi-decadal atmospheric GCM simulations. *International Journal of Climatology* **17**: 1263–1284.

Deser C, Blackmon ML. 1993. Surface climate variations over the North Atlantic Ocean during winter: 1900–1989. *Journal of Climate* **6**: 1743–1753.

Diaz HF, Hoerling MP, Eischeid JK. 2001. ENSO variability, teleconnections and climate change. *International Journal of Climatology* **15**: 1845–1862.

Dong B, Sutton RT, Jewson SP, O'Neill A, Slingo JM. 2000. Predictable winter climate in the North Atlantic sector during the 1997–1999 ENSO cycles. *Geophysical Research Letters* **27**: 985–988.

Enfield DB, Mayer DA. 1997. Tropical Atlantic sea surface temperature variability and its relationship to the El Nino southern oscillation. *Journal of Geophysical. Research* **102**: 929–945.

Feddersen H. 2000. Impact of global seas surface temperature on summer and winter temperatures in Europe in a set of seasonal ensemble simulations. *Quarterly Journal of the Royal Meteorological Society* **126**: 2089–2109.

Fovell RG, Fovell MYC. 1993. Climate zones of the conterminous United States defined using cluster analysis. *Journal of Climate* **6**: 2103–2135.

Fraedrich K. 1990. European Grosswetter during the warm and cold extremes of the El Niño southern oscillation. *International Journal of Climatology* **10**: 21–31.

Fraedrich K. 1993. An ENSO impact on Europe? A review. *Tellus A* **46**: 540–552.

Fraedrich K, Muller K. 1992. Climate anomalies in Europe associated with ENSO extremes. *International Journal of Climatology* **12**: 25–31.

Gershunov A, Barnett TP. 1998. Interdecadal modulation of ENSO teleconnections. *Bulletin of the American Meteorological Society* **79**: 2715–2723.

Gershunov A, Schneider N, Barnett T. 2001. Low-frequency modulations of the ENSO-Indian monsoon rainfall relationship: signal or noise? *Journal of Climate* **14**: 2486–2492.
Giannini A, Cane MA, Kushnir Y. 2001. Interdecadal changes in the ENSO teleconnection to the Caribbean region and the North Atlantic oscillation. *Journal of Climate* **14**: 2867–2879.
Gong X, Richman MB. 1995. On the application of cluster analysis to growing season precipitation data in North America east of the Rockies. *Journal of Climate* **8**: 897–931.
Gouirand I, Moron V. 2000. Variabilité intra-saisonnière et multi-décennale de la téléconnexion entre les pressions de surface (100 °W–50 °E; 30°–70 °N) et les ENSO/LNSO (1873–1996). *Comptes Rendus de l'Academie des Sciences, Série IIa* **331**: 633–641.
Halpert MS, Ropelewski CF. 1992. Surface temperature patterns associated with the southern oscillation. *Journal of Climate* **5**: 577–593.
Hamilton K. 1988. A detailed examination of the extratropical response to tropical El Niño southern oscillation events. *Journal of Climatology* **8**: 67–86.
Hannachi A. 2001. Toward a non-linear identification of the atmospheric response to ENSO. *Journal of Climate* **14**: 2138–2149.
Hoerling MP, Kumar A, Zhong M. 1997. El Niño, La Niña and the nonlinearity of their teleconnections. *Journal of Climate* **10**: 1769–1785.
Honda M, Nakamura H, Ukita J, Kousaka I, Takeuchi K. 2001a. Interannual seesaw between the Aleutian and Icelandic lows. Part I: seasonal dependence and life cycle. *Journal of Climate* **14**: 1029–1042.
Honda M, Nakamura H, Ukita J, Kousaka I, Takeuchi K. 2001b. Interannual seesaw between the Aleutian and Icelandic lows. Part II. Its significance in the interannual variability over the wintertime Northern Hemisphere. *Journal of Climate* **14**: 4512–4529.
Huang J, Higuchi Y, Shabbar K. 1998. The relationship between the North Atlantic oscillation and the El Niño southern oscillation. *Geophysical Research Letters* **25**: 2707–2710.
Hurrell JW. 1995. Decadal trends in the North Atlantic oscillation: regional temperatures and precipitation. *Science* **269**: 676–679.
Hurrell JW, van Loon H. 1997. Decadal variations in climate associated with the North Atlantic oscillation. *Climate Change* **36**: 301–326.
Kiladis GN, Diaz HF. 1989. Global climatic anomalies associated with extremes of the southern oscillation. *Journal of Climate* **2**: 1069–1080.
Kumar A, Hoerling MP. 1997. Interpretation and implications of the observed inter-El Niño variability. *Journal of Climate* **10**: 83–91.
Kumar A, Hoerling MP. 1998. Annual cycle of Pacific–North American seasonal predictability associated with different phases of ENSO. *Journal of Climate* **11**: 3295–3308.
Kushnir Y. 1994. Interdecadal variations in North Atlantic sea surface temperature and associated atmospheric conditions. *Journal of Climate* **7**: 141–157.
Lau NC. 1997. Interactions between global SST anomalies and the midlatitude atmospheric circulation. *Bulletin of the American Meteorological Society* **78**: 21–34.
Lau NC, Nath MJ. 2001. Impact of ENSO in SST variability in the North Pacific and North Atlantic seasonal dependence and role of extratropical sea air coupling. *Journal of Climate* **14**: 2846–2865.
Lee EJ, Jhun JG, Kang IS. 2002. The characteristic variability of boreal wintertime atmospheric circulation in El Niño events. *Journal of Climate* **15**: 892–904.
Marshall J, Kushnir Y, Battisti D, Chang P, Czaja A, Dickson R, Hurrel J, McCartney M, Saranavan R, Visbeck M. 2001. North Atlantic climate variability: phenomena, impacts and mechanisms. *International Journal of Climatology* **21**: 1863–1898.
May W, Bengtsson L. 1998. The signature of ENSO in the Northern Hemisphere midlatitude seasonal mean flow and high-frequency intraseasonal variability. *Meteorology and Atmospheric Physics* **69**: 81–100.
Moron V, Ward MN. 1998. ENSO teleconnection with climate variability in the European and African sectors. *Weather* **53**: 287–295.
Moron V, Gouirand I. 2003. Seasonal modulation of the ENSO relationship with sea level pressure anomalies over the North Atlantic in October–March 1873–1996. *International Journal of Climatology* **23**: 143–155.
Moron V, Plaut G. 2003. The impact of ENSO on weather regimes over North Atlantic and Europe during boreal winter. *International Journal of Climatology* **23**: 363–379.
Moron V, Navarra A, Ward MN, Folland CK, Friederichs P, Polcher J, Maynard K. 2001. Analysing and combining atmospheric general circulation model simulations forced by prescribed SST. Part II: northern extratropical response. *Annali di Geofisica* **44**: 781–794.
Peng S, Robinson WA, Li S. 2002. North Atlantic SST forcing of the NAO and relationships with intrinsic hemispheric variability. *Geophysical Research. Letters* **29**: 117/1–117/4.
Philander SGH. 1990. *El Niño, La Niña and the Southern Oscillation*. Academic Press: San Diego.
Portis DH, Walsh JE, El Hamly M, Lamb PJ. 2001. Seasonality of the North Atlantic oscillation. *Journal of Climate* **14**: 2069–2078.
Pozo-Vazquez D, Esteben-Parra MJ, Rodrigo FS, Castro-Diez Y. 2001. The association between ENSO and winter atmospheric circulation and temperature in the North Atlantic region. *Journal of Climate* **14**: 3408–3420.
Raible CC, Luksch U, Fraedrich K, Voss R. 2001. North Atlantic decadal regimes in a coupled GCM simulation. *Climate Dynamics* **18**: 321–330.
Robock A. 2000. Volcanic eruptions and climate. *Reviews in Geophysics* **38**: 191–219.
Rocha A. 1999. Low-frequency variability of seasonal rainfall over the Iberian Peninsula and ENSO. *International Journal of Climatology* **19**: 889–902.
Rodo X, Baert E, Comin FA. 1997. Variations in seasonal rainfall in southern Europe during the present century: relationships with the North Atlantic oscillation and ENSO. *Climate Dynamics* **13**: 275–284.
Rogers JC. 1984. The association between the North Atlantic oscillation and the southern oscillation in the Northern Hemisphere. *Monthly Weather Review* **112**: 1999–2015.
Ropelewski CF, Halpert MS. 1987. Global and regional precipitations patterns associated with the ENSO. *Monthly Weather Review* **115**: 1606–1626.
Ropelewski CF, Halpert MS. 1989. Precipitations patterns associated with the high phase of the southern oscillation. *Journal of Climate* **2**: 268–284.
Ropelewski CF, Halpert MS. 1996. Quantifying SO–precipitation relationships. *Journal of Climate* **9**: 1043–1059.

Shabbar A, Higuchi K, Skinner W, Knox J. 1997. The association between the BWA index and winter surface temperature variability over eastern Canada and west Greenland. *International Journal of Climatology* **17**: 1195–1210.
Shukla JG, Paolino DA, Straus DM, De Witt D, Fennessy M, Kinter JL, Marx L, Mo R. 2000. Dynamical seasonal predictions with the COLA atmospheric model. *Quarterly Journal of the Royal Meteorological Society* **126**: 2265–2291.
Slonosky V, Yiou P. 2002. Does the NAO index represent zonal flux? The influence of the NAO on the North Atlantic sea surface temperature. *Climate Dynamics* **19**: 17–30.
Smith SR, Green PM, Leonardi AP, O'Brien JJ. 1998. Role of multiple-level tropospheric circulations in forcing ENSO winter precipitation anomalies. *Monthly Weather Review* **124**: 3102–3116.
Straus DM, Shukla JG. 2000. Distinguishing between the SST-forced variability and internal variability in mid-latitudes: analysis of observations and GCM simulations. *Quarterly Journal of the Royal Meteorological Society*. **126**: 2323–2350.
Sutton RT, Hodson DLR. 2003. Influence of the ocean on North Atlantic climate variability (1871–1999). *Journal of Climate*: submitted for publication.
Terray L, Cassou C. 2002. Tropical Atlantic sea surface temperature forcing of quasi-decadal climate variability over the North Atlantic–European region. *Journal of Climate* **15**: 3170–3187.
Thompson DWJ, Wallace JM. 1998. The Arctic oscillation signature in the wintertime geopotential height and temperature fields. *Geophysical Research Letters* **25**: 1297–1300.
Van Oldenborgh GJ, Burgers G, Klein Tank A. 2000. On the El Niño teleconnection to spring precipitation in Europe. *International Journal of Climatology* **20**: 565–573.
Venzke R, Allen M, Sutton RT, Rowell D. 1998. The atmospheric response over the North Atlantic to decadal changes in sea surface temperature. *Journal of Climate* **12**: 2562–2584.
Von Storch H, Zwiers FW. 1998. *Statistical Analysis in Climate Research*. Cambridge University Press: New York.
Wallace JM, Gutzler DS. 1981. Teleconnections in the geopotential height field during the Northern Hemisphere winter. *Monthly Weather Review* **109**: 784–812.
Wallace JM, Thompson DWJ. 2002. The Pacific center of action of the Northern Hemisphere annular mode: real or artifact? *Journal of Climate* **15**: 1987–1991.
Yulaeva E, Wallace JM. 1994. Signature of ENSO in global temperature and precipitation fields derived from the microwave sounding unit. *Journal of Climate* **7**: 1719–1736.
Zorita E, Kharin V, von Storch H. 1992. The atmospheric circulation and sea surface temperature in the North Atlantic area in winter: their interaction and relevance for Iberian Peninsula. *Journal of Climate* **5**: 1097–1108.

